# Modeling Bare Soil L-Band Polarimetric $H$-$\alpha$ Values Using a Second-Order SPM Model

Natalia Soledad Morandeira, *Member, IEEE*, Mariano Franco, Matías Barber, *Member, IEEE*, and Francisco Grings, *Member, IEEE*

***Abstract*—Polarimetric soil moisture retrieval is among the main objectives of leading synthetic-aperture-radar satellite missions since it allows to systematically analyze costly-to-obtain polarization information to increase retrieval accuracy. In this letter, we present the results of modeling the L-band entropy $(H)$ and alpha $(\alpha)$ values as a function of soil dielectric constant and roughness using a second-order small-perturbation model to simulate the polarimetric soil backscattering. Modeling results are then compared to bare soil uninhabited aerial vehicle synthetic aperture radar (UAVSAR) data acquired simultaneously to *in situ* field campaigns in Canada during SMAPVEx12. Our model is able to correctly predict observed ranges of $H$ and $\alpha$ and to consistently model dielectric constant and roughness changes. Nevertheless, a systematic overestimation of $\alpha$ is observed when compared with the analyzed UAVSAR data set. Taking UAVSAR data as benchmark, theoretical reasons for this mismatch are analyzed.**

***Index Terms*—Synthetic aperture radar (SAR) polarimetry, soil moisture, uninhabited aerial vehicle synthetic aperture radar (UAVSAR).**

## I. Introduction

THE amount of moisture inside the soil over agricultural lands is a key variable related to crop development and yield. Too much or too little moisture can each have devastating effects: persistently dry soil causes plants to wilt and diminishes their ability to transpire and grow. By contrast, excess moisture results in poor seed germination, inadequate nutrient uptake, and soil compaction. Consequently, monitoring moisture changes is particularly important prior to—and throughout—the seeding season [1].

However, the retrieval of high resolution soil moisture of bare soils using remote sensing data is still a challenge due to several reasons. First, although, in principle, the polarimetric backscattering coefficient $(\sigma^0)$ measured by synthetic aperture radars (SARs) is sensitive to soil moisture, the relation between them is complex and soil dependent. Second, agricultural soil moisture presents large spatiotemporal variability.

Manuscript received November 11, 2015; revised December 17, 2015; accepted December 31, 2015. Date of publication January 28, 2016; date of current version February 24, 2016.

N. S. Morandeira is with the Laboratorio de Ecología, Teledetección y Ecoinformática, Instituto de Investigación e Ingeniería Ambiental, Universidad Nacional de San Martín, B1650HMP General San Martín, Argentina and also with the Consejo Nacional de Investigaciones Cientcas y Técnicas (CONICET), Buenos Aires, Argentina.

M. Franco, M. Barber, and F. Grings are with the Instituto de Astronomía y Física del Espacio (IAFE, CONICET-UBA), C1428ZAA Buenos Aires, Argentina (e-mail: verderis@iafe.uba.ar).

Color versions of one or more of the figures in this paper are available online at http://ieeexplore.ieee.org.

Digital Object Identifier 10.1109/LGRS.2016.2516502

The first issue is usually tackled using physically based interaction models, which calculate soil backscattering as a function of soil parameters [i.e., volumetric soil moisture content $m_v$ [cm$^3$ /cm$^3$], soil surface roughness $s$, and soil surface autocorrelation function (ACF)]. These models are characterized by a set of hypothesis, related to the medium and the electromagnetic fields over the air/soil interface.

Typical soil moisture retrieval schemes are based on the direct comparison between modeled and observed $\sigma^0_{pq}$ (where $p$, $q$ stands for $H$, $V$ polarizations): The retrieved values are the set of $(m, s)$ parameters which better fits the observed $\sigma^0_{pq}$ according to the model. However, by using only the radar cross sections, these retrieval schemes do not exploit the full polarimetric information contained in the radar data (particularly, the phase between polarization channels). Moreover, all three channels ($\sigma^0_{hh}$, $\sigma^0_{hv}$, and $\sigma^0_{vv}$) increase for increasing values of $m$ and $s$, and therefore, there is a strong correlation among the information provided by the SAR system for this application. This is particularly relevant in a retrieval scheme in which the discrepancies between model outputs and observations in every channel contribute equally to the overall retrieval error.

To fully exploit the information available, it is desirable to perform the retrieval over parameters with the following characteristics: 1) parameters that integrate the available polarimetric information by taking into account the expected physical constraints (e.g., reciprocity); 2) parameters that are polarization basis invariant; and 3) parameters that summarize the total level of depolarization and the average polarized information [2]. The entropy $(H)$-alpha $(\alpha)$ polarization decomposition fits this criterion and provides a robust theoretical framework for SAR-based soil moisture retrieval.

Several examples of such a scheme are available in the literature [3]–[5]. In them, $H$ and $\alpha$ values are computed using different versions of the small-perturbation model, and its retrieval performance is evaluated using *in situ* data. In general, the results are mixed, and there is a lack of direct comparison between modeled and observed $H$ and $\alpha$ values.

In this letter, we modeled the $H$ and $\alpha$ values using a second-order small perturbation (SPM-2) approximation to simulate the polarimetric soil backscattering. Next, the results were compared to uninhabited aerial vehicle synthetic aperture radar (UAVSAR) data acquired in Canada over bare soils, which provide a reliable data set against to test the simulation results. From the comparison, we showed the limitations of current approaches to model real $H$ and $\alpha$ values and extended the validity region by using the SPM-2 model. To discuss the concordance or mismatches between the models and ground-truth data, we used *in situ* soil permittivity and roughness data obtained simultaneously to UAVSAR acquisition. Finally, we present some conclusions about the modeling exercise.

## II. Scattering Model: Second-Order Small Perturbation

The small-perturbation method (SPM) allows to compute the polarimetric soil backscattering as a function of soil dielectric constant ($\epsilon$) and soil profile roughness characteristics. As its name indicates, the main approximation is that the incident wavelength should be larger than the surface height ($ks \ll 0.3$, where $k = 2\pi/\lambda$) [6]–[9]. When this condition is satisfied, the scattered fields can be computed using a perturbative series in the surface heights. The strategy is to find the unknown amplitudes of the scattered and transmitted fields using the boundary conditions of the Maxwell equations. These equations are written as a power series in the surface heights and are solved in an iterative way up to the desired order. The first-order results are well known and get to the Bragg scattering reflection coefficients. Although this solution is easy to obtain, it leads to zero cross-polarization and does not ensure energy conservation. A solution up to the second order in the surface heights is necessary to avoid these two issues.

The basic formulation of the SPM is as follows: First, the scattered field is written in terms of the unknown amplitudes $\alpha$ and $\beta$

$$\mathbf{E}^s = \int \frac{d^2k_\perp}{(2\pi)^2}[\alpha\ \hat{h}_s + \beta\ \hat{v}_s]\ e^{\imath \mathbf{k}_\perp \cdot \mathbf{r}}\ e^{\imath k_{zs}\ z} \tag{1}$$

where $\mathbf{r} = (x, y)$ and $z = f(\mathbf{r})$. The polarization of the scattered field is provided by the $\hat{h}_s$ and $\hat{v}_s$ vectors. The vertical component of the wavenumber is $k_{zs} = \sqrt{k_0^2 - k_\perp^2}$, with $k_0 = 2\pi/\lambda$ being the incident wavenumber. A similar formulation is done for the transmitted field, which introduces two more unknown amplitudes.

Next, an expansion series is proposed for both the unknown amplitudes and the exponential factor that depends on $z(\mathbf{r})$. Hence, we have terms of the kind

$$\alpha\ \hat{h}_s\ e^{\imath k_{zs}\ z} \approx \left[\alpha^{(0)} + \alpha^{(1)} + \alpha^{(2)} + \cdots\right] \times \left[1 + \imath\ k_{zs}\ z + \frac{1}{2}\imath^2\ (k_{zs}\ z)^2 + \cdots\right]\ \hat{h}_s. \tag{2}$$

Through the boundary conditions for the tangential fields over the illuminated area, it is given a complete set of relations to find the unknown amplitudes of the scattered and transmitted fields. In this letter, we follow the solution found by Johnson [9]. Up to the second order and considering only the scattered field (the only one relevant for this case), the unknown amplitudes take the form

$$\alpha(\mathbf{k}_\perp) \approx \alpha^{(0)}\ \delta(\mathbf{k}_\perp - \mathbf{k}_{i\perp}) + \alpha^{(1)}\ \mathcal{Z}(\mathbf{k}_\perp) + \int d^2k'_\perp\ \alpha^{(2)}\left(\mathbf{k}_\perp, \mathbf{k}'_\perp\right)\ \mathcal{Z}\left(\mathbf{k}_\perp - \mathbf{k}'_\perp\right) \tag{3}$$

and a similar expression is obtained for the amplitude $\beta$. We have a set of parameters $\{\alpha^{(n)},\ \beta^{(n)}\}$ for the transverse electric (TE) mode and a different set for the transverse magnetic (TM) mode (see [9]).

These amplitudes have a ready interpretation. The zeroth-order term gives the specular reflection, and it is proportional to the Bragg reflection coefficient. The first-order coefficient is a single scattering term that depends only on the Fourier transform of the surface ($\mathcal{Z}(\mathbf{k})$) evaluated at a single mode. The second-order term shows the multiple scattering process through the integration of an auxiliary mode in $\mathcal{Z}$.

If, for example, we want to obtain the HH channel, we should compute the product between the aforementioned expression and the $\hat{h}_s$ direction. Then, the scattered field will be proportional only to the $\alpha_h^{(n)}$ terms, where the subscript $h$ points out that the incident field is in the TE mode. In the same way, the VV channel is given by the $\beta_v^{(n)}$ coefficients, and the HV channel is given by the set $\beta_h^{(n)}$.

To compute the mean values needed in the coherency matrix, showed in (6), we replace (3) in (1). Schematically, the computed terms are

$$\begin{aligned}\left\langle E^s_{qq}\ E^{s^*}_{pp}\right\rangle = {} & \psi_q^{(0)}\ \psi_p^{(0)^*} + \psi_q^{(1)}\ \psi_p^{(1)^*} \int d^2k'_\perp\ \mathcal{W}\left(\mathbf{k}_\perp - \mathbf{k}'_\perp\right) \\ & + \int d^2k'_\perp \left[\psi_q^{(0)}\ \psi_p^{(2)^*} + \psi_p^{(0)^*}\ \psi_q^{(2)}\right]\ \mathcal{W}(\mathbf{k}_\perp - \mathbf{k}'_\perp) \\ & + 2\int d^2k'_\perp\ \psi_q^{(2)}\ \mathcal{W}\left(\mathbf{k}_{i\perp} - \mathbf{k}'_\perp\right) \int d^2k''_\perp\ \psi_p^{(2)^*} \\ & \times \mathcal{W}\left(\mathbf{k}_{i\perp} - \mathbf{k}''_\perp\right) \\ & + \int d^2k'_\perp \int d^2k''_\perp\ \psi_q^{(2)}\ \psi_p^{(2)^*}\ \mathcal{W}\left(\mathbf{k}_{i\perp} - \mathbf{k}'_\perp\right) \\ & \times \mathcal{W}\left(\mathbf{k}'_\perp - \mathbf{k}''_\perp\right).\end{aligned} \tag{4}$$

In the aforementioned equation, $\psi^{(n)}$ represents the coefficients of the scattered field, and $\mathcal{W}(\mathbf{k})$ is the roughness spectrum of the surface

$$\mathcal{W}(\mathbf{k}_\perp) = \int \frac{d^2r}{(2\pi)^2}\ C\left(|\mathbf{r}|\right)\ e^{\imath \mathbf{r}\cdot\mathbf{k}_\perp} = \frac{s^2\ l^2}{4\ \pi}\ e^{-\frac{1}{4}l^2\ \mathbf{k}_\perp^2} \tag{5}$$

where $C(|\mathbf{r}|)$ is a Gaussian ACF, $s$ [cm] is the mean height, and $l$ [cm] is the correlation length.

All the terms involved in the coherency matrix are computed by properly using (4). To obtain the mean value of the HH channel, the $\psi$ coefficients have to be changed by the $\alpha_h$ ones. To calculate the mean value of the product between the HH and VV channels, $\psi_q$ needs to be changed by $\alpha_h$, and $\psi_p^*$ needs to be changed by $\beta_v^*$. By this procedure, all the elements of the coherence matrix shown in (6), shown at the bottom of the page, can be computed.

$$T = \begin{bmatrix} \left\langle |S_{HH} + S_{VV}|^2 \right\rangle & \left\langle (S_{HH} + S_{VV})\ (S_{HH} - S_{VV})^* \right\rangle & 2\left\langle (S_{HH} + S_{VV})\ S^*_{HV} \right\rangle \\ \left\langle (S_{HH} + S_{VV})^*\ (S_{HH} - S_{VV}) \right\rangle & \left\langle |S_{HH} - S_{VV}|^2 \right\rangle & 2\left\langle (S_{HH} - S_{VV})\ S^*_{HV} \right\rangle \\ 2\left\langle (S_{HH} + S_{VV})^*\ S_{HV} \right\rangle & 2\left\langle (S_{HH} - S_{VV})^*\ S_{HV} \right\rangle & 4\left\langle |S_{HV}|^2 \right\rangle \end{bmatrix} \tag{6}$$

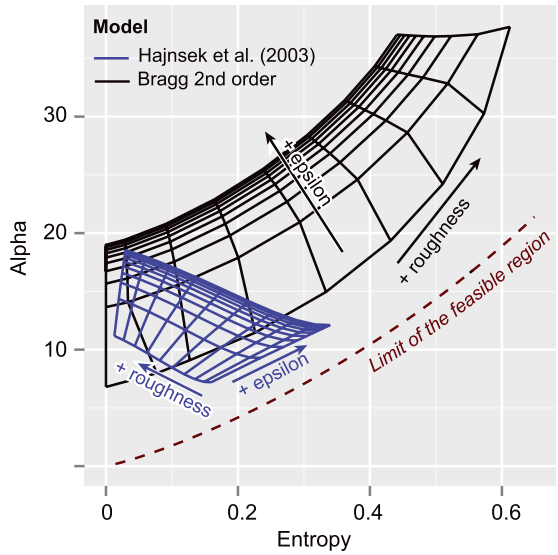


Fig. 1. Simulated $H$ and $\alpha$ values as a function of $\epsilon$ and roughness for the SPM-0 (see [3]) and SPM-2 models. Roughness is described as the width of the rotation angle distribution around local surface slopes in the former and as the soil RMS height $s$ in the latter (Gaussian ACF, $l = 10$ cm). Results are for $2 < \epsilon < 40$, $0$ cm $< s < 1.5$ cm, $\lambda = 0.25$ cm (L-band), and $\theta = 40°$ (the mean UAVSAR incident angle for the plots was $\theta = 36°$).

### A. *Scattering Model Simulations*

Previous studies have followed similar approaches and computed $H$ and $\alpha$ from scattering models in order to estimate the soil relative dielectric constant $\epsilon$ from polarimetric SAR data. In particular, the authors of [3] and [4] have used the zero-order solution of the SPM (SPM-0) and a rotation symmetry argument of the T matrix to compute $H$ and $\alpha$ and then retrieve $m$ from L-band E-SAR (DLR) airborne experimental SAR system and University of Michigan truck-mounted polarimetric scatterometer data.

Fig. 1 presents the main results of the two modeling approximations. The SPM-0 model predicts an increase in both $H$ and $\alpha$ for increases in soil $\epsilon$ and a radial pattern for the soil roughness (width of the distribution of the aspect parameter; see [3]). Since the SPM model quickly saturates for $\epsilon > 20$, the model spans a limited range of the H-$\alpha$ plane ($H < 0.35$, $\alpha < 20°$).

The results presented in this letter (SPM-2) present a very different pattern. Specifically, iso-$\epsilon$ lines now lay more or less parallel to the $H - \alpha$ limit of the feasible region. Moreover, for the same range of $\epsilon$, the SPM-2 model spans a larger area of the $H - \alpha$ plane ($H < 0.6$, $\alpha < 40°$), indicating an enhanced sensitivity to dielectric constant and roughness. For this model, $H$ increases when the surface becomes rougher, as expected (see [10, Ch. 2.4]). The SPM-2 model reaches values of entropy close to 0.5 in the limit of validity of the scattering model (i.e., $s = 1.5$ cm, for L-band). This range in $H$ is in closer agreement with the one observed with UAVSAR observations, as we will show later.

The observed differences (H-$\alpha$ pattern as a function of $\epsilon$ and $s$ and range in the H-$\alpha$ plane) are related to several factors. From the theoretical point of view, the primarily difference is related to the first- and second-order terms of the model, which ensure energy conservation and consider multiple scattering, effects that lead to nonzero $\sigma^0_{HV}$ values. Since the modeled $\sigma^0_{HV}$ values are low in comparison with modeled co-pol terms, they will have low impact in the retrieval of $\epsilon$ based on direct minimization schemes of polarimetric channels. On the contrary, it is highly relevant in polarimetric analysis, in which nonzero modeled $\sigma^0_{HV}$ implies five nonzero terms of the $T$ matrix, which themselves lead to nonzero and physically coherent H values.

Moreover, in the approach of this letter, roughness is modeled via its ACF ($\mathcal{W}$), while in [3], it is introduced by assuming a distribution of scatterers with different aspect angles. This implies that, in the latter approach, $\sigma^0_{HV}$ is "synthesized" by assuming scatterers with different aspect angles, whose distribution is loosely related to soil roughness. On the contrary, in the approach presented here, the soil profile root mean square (RMS) height $s$ is a physically measurable roughness parameter which is used as an input parameter of the ACF.

## III. Available Data

A geocodified UAVSAR scene (L-band acquisition date of June 17, 2012, flight line ID 31605, and flight request ID 12G003) was imported to PolSARpro version 5.0 [11]. Single polarizations (HH, HV, VV) were derived from the covariance matrix and transformed to decibels. UAVSAR data are preprocessed with 3 range looks and 12 azimuth looks. The coherence matrix was filtered to reduce speckle noise with an adaptive refined Lee filter ($3 \times 3$ pixel window size) [12]. The entropy $(H)$ and mean alpha angle $(\alpha)$ components of the Cloude–Pottier decomposition [2] were extracted with a window size of $5 \times 5$ pixels, thus reducing even more the effect of speckle noise. Thus, the equivalent number of looks with which $(H)$ and $(\alpha)$ are computed is higher than 50, so we assume that the extracted parameters are nonbiased [13]. It is worthwhile to mention that UAVSAR data are calibrated taking into account polarization effects, with absolute radiometric calibration bias $\sim$1 dB, residual RMS errors of $\sim$0.7 dB, and RMS phase errors $\sim$5.3° [14].

Fifteen agricultural fields in the UAVSAR scene were analyzed. These fields were in bare soil condition (volume water content $< 0.2$ kg/m$^2$) and with simultaneous *in situ* data (dielectric constant and roughness) [15]. Regions of interest were drawn onto each field, avoiding edges, trails, and other sources of heterogeneity. Backscattering values for the single polarizations were extracted for each of the fields [see Fig. 2(b)–d)].

Based on these results and on visual inspection, four fields were removed from further analyses to avoid including flashing fields (fields 14, 103, 111, and 112). Two other fields were removed due to their high backscattering heterogeneity (field 102) or because of relatively large $\sigma^0_{HV}$, possibly indicating the presence of vegetation or vegetation residue (field 123). The remaining nine fields were relatively homogeneous but differed in their dielectric constants [see Fig. 2(a)]. For all but one of the fields, *in situ* measurements were acquired on June 17, 2012, simultaneously with SAR acquisition; for the remaining field, the *in situ* measurements were done on June 15, 2012. Available per-field dielectric constant values for these two days (48 to 96 measurements per field) were averaged.

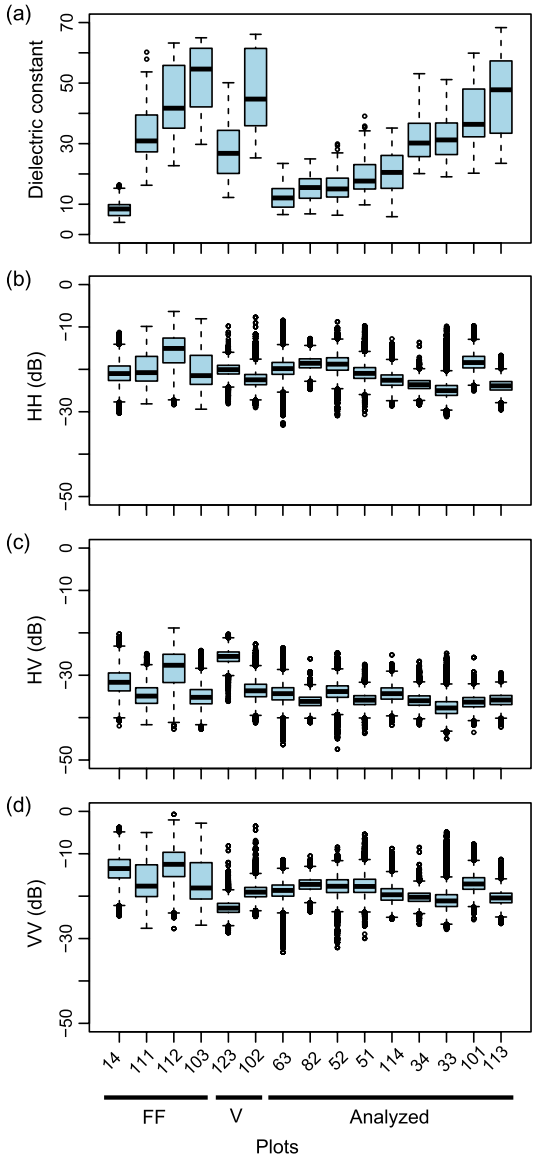


Fig. 2. Analyzed bare soil fields in the UAVSAR scene (L-band) acquired on June 17, 2012 (flight line ID 31605). In the first four fields, flashing fields (marked as FF) were observed [16]. Plots 123 and 102 were highly heterogeneous, probably vegetated, and were excluded from further analyses (marked as V). The remaining fields are ordered with increasing dielectric constant values. (a) Dielectric constant values of the fields, measured with handheld probes in the SMAPVEx12 experiment. Roughness values were reported constant, $s \sim 1$ cm [15]. (b) $\sigma^0_{HH}$. (c) $\sigma^0_{HV}$. (d) $\sigma^0_{VV}$.

### A. Results

Observed $H$ and $\alpha$ values were compared in the $H/\alpha$ space with the SPM-0 and SPM-2 model simulations (see Fig. 3).

Several observations are in order. First, all the fields are located inside the low $H$–low $\alpha$ zone in the $H$-$\alpha$ plane corresponding to isotropic surface scatterers. Second, only two fields are in the expected range of the SPM-0 model (fields 82 and 101), while five fields are in the expected range of the SPM-2 model (fields 51, 114, 33, 34, and 113). Third, intrafield $H-\alpha$ variation is mainly in the direction of the $H-\alpha$ line that limits the feasible region of the $H-\alpha$ plane. Fourth, fields 52 and 63 present very low values of $\alpha$ and medium values of $H$, which are not well represented by any of these two models. Fifth, although spanning a larger area of the $H-\alpha$ plane, the SPM-2 model overestimates bare soil $\alpha$ values for a given *in situ* dielectric constant (results not shown, but obvious from the comparison of Figs. 1 and 3; note that the first iso-$\epsilon$ line corresponds to $\epsilon = 2$). This implies that, although inside the model range, predicted $\epsilon$ values for this plots are much lower than the ones measured in the field. Finally, flashing fields present large $\alpha$ values and medium H values, characteristics that are unusual for bare soils.

## IV. Discussion

In this letter, the results of comparing UAVSAR data with two models for $H-\alpha$ (a zero- and a second-order SPM model) were presented. Due to their overall quality, UAVSAR data can be considered as highly reliable and can be used to test these two modeling approaches [14]. As seen, the SPM-0 model spans a very small portion of the $H-\alpha$ plane, which does not overlap with the L-band experimental data. On the contrary, the SPM-2 model spans almost the same range of the experimental data in both $H$ and $\alpha$, although there is a systematic overestimation of $\alpha$ (for a given measured value of $\epsilon$), which will lead to a poor retrieval [although *in situ* $\epsilon$ presented very large variances; see Fig. 2(a)].

The main difference among model simulation results is the inversion of the direction of the iso-$\epsilon$ lines between the models. In particular, iso-$\epsilon$ for SPM-2 now lies parallel to the $H-\alpha$ azimuthal symmetry line (which delimits the $H-\alpha$ plane feasible region for any scatterer). Therefore, according to the predictions derived from the SPM-2 model, an increase in $H-\alpha$ values in a direction parallel to this azimuthal symmetry line will be related to an increase in soil roughness (for bare soils). According to this interpretation, the observed intrafield $H-\alpha$ variability is mainly the intrafield roughness variability. This is also consistent with the fact that the $H-\alpha$ azimuthal symmetry line is theoretically generated by increasing the depolarization factor of an azimuthally symmetric target [2]. This increase in depolarization is consistent with the effects of an increase in roughness (which, according to interaction models, leads to an increase in $\sigma^0_{HV}$ and a decrease in $\sigma^0_{HH}-\sigma^0_{VV}$).

The single factor that severely limits the applicability of this model to bare soil moisture retrieval is its systematic overestimation of $\alpha$ for a measured $\epsilon$ value. Indeed, observed UAVSAR data presents values of $\alpha$ which are $\sim 10^\circ$ lower than SPM-2 model predictions for a given value of $\epsilon$ (according to a retrieval made using the SMP-2 model, neither of the studied plots should have a value of $\epsilon$ larger than 12). Excluding uncertainties in field data, this overestimation is probably related to two facts: an underestimation of soil $\sigma^0_{HV}$ and the definition of the reflection coefficients. The first is probably related to unaccounted complex scattering mechanisms inside the soil (volume scattering) and higher order surface scattering. The former is probably related to the definition of the Bragg reflection coefficients that lead to the same sign but relatively large values of $\sigma^0_{HH}-\sigma^0_{VV}$ (even for low values of $\epsilon$), which leads to relatively large values of $\alpha$. As $\epsilon$ increases, so does the difference between $\sigma^0_{HH}-\sigma^0_{VV}$ and $\alpha$.

The estimation of soil moisture from properly calibrated polarimetric SAR data using polarimetry techniques is promissory since it automatically takes into account relevant physical constraints in the radar data. However, it poses a challenge to soil scattering modeling since it requires physically

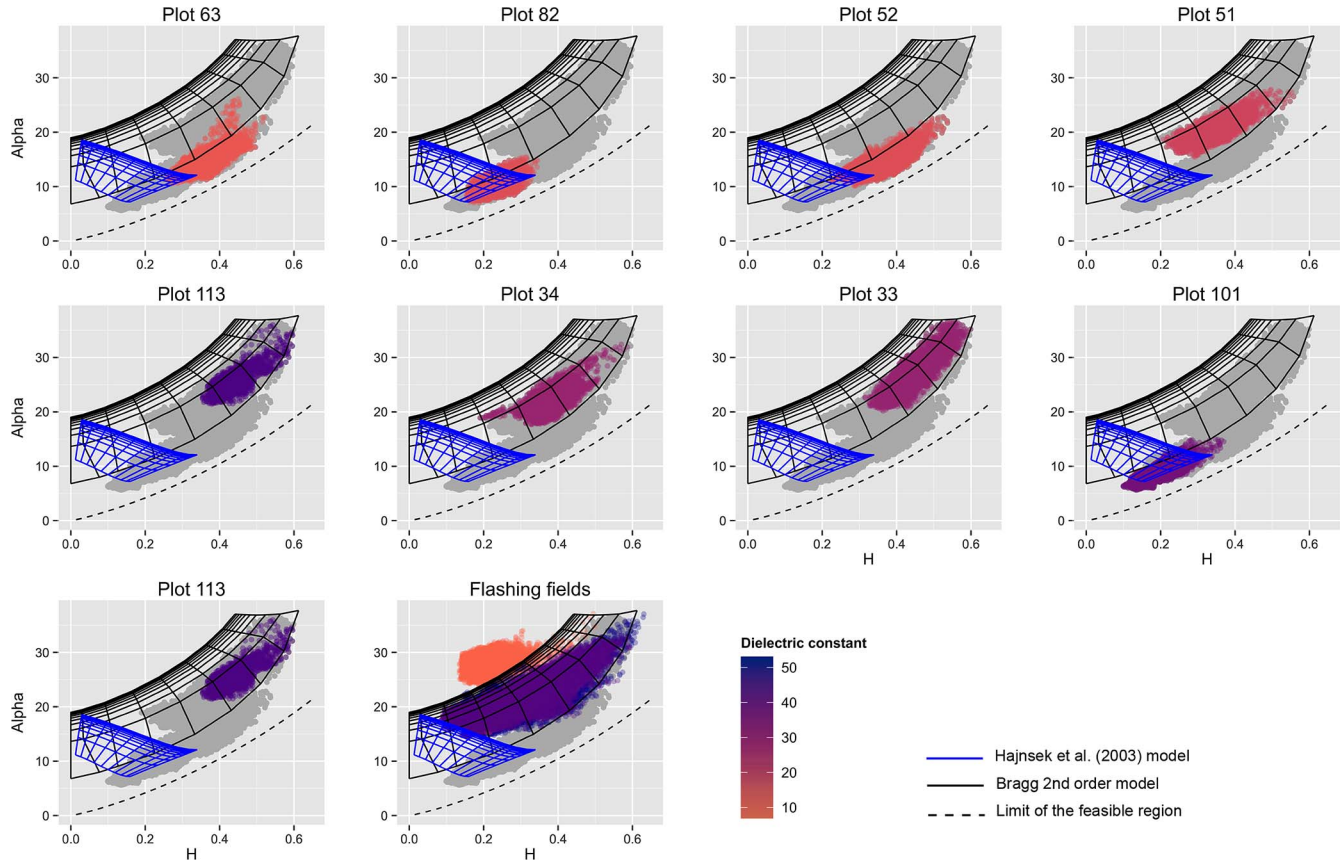


Fig. 3. Distribution of the UAVSAR data of each of the analyzed SMAPVEx12 fields in the $H - \alpha$ space. Plots were ordered with increasing dielectric constant values [see Fig. 2(a)]. Models correspond to those plotted on Fig. 1. Flashing fields were included as reference. In each plot, the gray area corresponds to the total data available, and the colored one corresponds to the different agricultural fields analyzed in every subplot.

based models that fit available polarimetric parameters (e.g., $H - \alpha$ data). In order to solve the main modeling issue encountered in this UAVSAR data set ($\alpha$ overestimation), we intend to use a two-layer model taking into account soil internal structure and therefore considering soil volume scattering (which should lead to an increase in $\sigma^0_{HV}$ and a consequent decrease in $\alpha$).

## ACKNOWLEDGMENT

The authors would like to thank H. McNairn (Science and Technology Branch, Agriculture and Agri-Food Canada, Ottawa, ON, Canada) for providing the SMAPVEx12 field data. The authors also thank the reviewers for their valuable feedback.

## REFERENCES

[1] H. McNairn, A. Merzouki, A. Pacheco, and J. Fitzmaurice, "Monitoring soil moisture to support risk reduction for the agriculture sector using RADARSAT-2," *IEEE J. Sel. Topics Appl. Earth Observ. Remote Sens.*, vol. 5, no. 3, pp. 824–834, Jun. 2012.

[2] S. R. Cloude and E. Pottier, "An entropy based classification scheme for land applications of polarimetric SAR," *IEEE Trans. Geosci. Remote Sens.*, vol. 35, no. 1, pp. 68–78, Jan. 1997.

[3] I. Hajnsek, E. Pottier, and S. Cloude, "Inversion of surface parameters from polarimetric SAR," *IEEE Trans. Geosci. Remote Sens.*, vol. 41, no. 4, pp. 727–744, Apr. 2003.

[4] A. Iodice, A. Natale, and D. Riccio, "Retrieval of soil surface parameters via a polarimetric two-scale model," *IEEE Trans. Geosci. Remote Sens.*, vol. 49, no. 7, pp. 2531–2547, Jul. 2011.

[5] I. Hajnsek, T. Jagdhuber, H. Schon, and K. Papathanassiou, "Potential of estimating soil moisture under vegetation cover by means of PolSAR," *IEEE Trans. Geosci. Remote Sens.*, vol. 47, no. 2, pp. 442–454, Feb. 2009.

[6] F. T. Ulaby, R. K. Moore, A. K. Fung, and A. House, *Microwave Remote Sensing: Active and Passive*, vol. 2. Reading, MA, USA: Addison-Wesley, 1981.

[7] A. G. Voronovich, *Wave Scattering From Rough Surfaces*. Berlin, Germany: Springer-Verlag, 1994.

[8] T. M. Elfouhaily and C.-A. Guérin, "A critical survey of approximate scattering wave theories from random rough surfaces," *Waves Random Media*, vol. 14, no. 4, pp. R1–R40, Oct. 2004.

[9] J. T. Johnson, "Third-order small-perturbation method for scattering from dielectric rough surfaces," *J. Opt. Soc. Amer. A, Opt. Image Sci.*, vol. 16, no. 11, pp. 2720–2736, Nov. 1999.

[10] S. Cloude, *Polarisation: Applications in Remote Sensing*. Oxford, U.K.: Oxford Univ. Press, 2009.

[11] PolSARpro. V. 5.0, European Space Agency, Paris, France, 2015.

[12] J.-S. Lee, "Speckle suppression and analysis for synthetic aperture radar images," *Opt. Eng.*, vol. 25, no. 5, May 1986, Art. ID 255636.

[13] C. Lopez-Martinez, A. Alonso-Gonzalez, and X. Fabregas, "Perturbation analysis of eigenvector-based target decomposition theorems in radar polarimetry," *IEEE Trans. Geosci. Remote Sens.*, vol. 52, no. 4, pp. 2081–2095, Apr. 2014.

[14] A. Fore *et al.*, "UAVSAR polarimetric calibration," *IEEE Trans. Geosci. Remote Sens.*, vol. 53, no. 6, pp. 3481–3491, Jun. 2015.

[15] H. McNairn *et al.*, "The Soil Moisture Active Passive Validation Experiment 2012 (SMAPVEX12): Prelaunch calibration and validation of the SMAP soil moisture algorithms," *IEEE Trans. Geosci. Remote Sens.*, vol. 53, no. 5, pp. 2784–2801, May 2015.

[16] U. Wegmuller, R. Cordey, C. Werner, and P. Meadows, "Flashing fields in nearly simultaneous ENVISAT and ERS-2 C-band SAR images," *IEEE Trans. Geosci. Remote Sens.*, vol. 44, no. 4, pp. 801–805, Apr. 2006.